MIKAILALSYS
Journal of Multidisciplinary Sciences

e-ISSN : 2987-2286
p-ISSN : 2987-3924

Index: Harvard, Boston, Sydney, Copernicus, Sinta 4, Scilit, Semantic, Google, etc

https://doi.org/10.58578/mikailalsys.v4i2.9251

Biodegradative Capability of Molecularly Identified *Pseudomonas fluorescens* Strains on Palm Oil-Polluted Soil

Bukola Margaret Popoola, Ayooluwa Afelumo, Oyindamola John Samson
Ajayi Crowther University, Oyo, Oyo State, Nigeria
bm.popoola@acu.edu.ng

Article Info:

Submitted:	Revised:	Accepted:	Published:
Feb 9, 2026	May 7, 2026	May 19, 2026	May 24, 2026

Abstract

Oil palm (*Elaeis guineensis*) is an important source of edible vegetable oil derived from the fruit mesocarp; however, oil extraction commonly generates wastewater and residues that may be discharged into the environment without adequate treatment. Because microorganisms can degrade organic contaminants in palm oil mill effluent and oil-contaminated matrices, this study aimed to evaluate the potential of *Pseudomonas fluorescens* for remediating palm oil-contaminated soil. Palm oil and *P. fluorescens* isolates were obtained from Fiditi Oil Mill and Ajayi Crowther University, respectively, in Oyo State, Nigeria. Uncontaminated soil, oil mill soil, and purposefully contaminated soil were used as experimental control samples, while four purposefully contaminated soil samples and four oil mill soil samples were treated with *P. fluorescens* under varying soil sterilization and tillage conditions. The isolate was identified using 16S rRNA gene sequence analysis, and a 12-week field bioremediation trial was conducted to assess microbial load and residual oil content. The 16S rRNA sequencing confirmed the isolate as *P. fluorescens* MN607218.1. Residual oil in tilled sterile purposefully contaminated soil decreased from 0.13 g on day 0 to 0.10 g by week 12, whereas the corresponding non-sterile soil showed a greater reduction to 0.07 g by week 12.

Mikailalsys is licensed under a Creative Commons Attribution-NonCommercial-ShareAlike 4.0 International License

These findings indicate that *P. fluorescens* can effectively degrade palm oil in contaminated soil, particularly under non-sterile conditions, and may serve as a promising microbial agent for environmental cleanup of palm oil-contaminated sites.

Keywords: Palm Oil; *Pseudomonas fluorescens*; Bioremediation; Contaminated Soil; Oil Degradation

INTRODUCTION

Palm oil mill effluent (POME), according to Islam *et al.* (2018), is frequently released straight from a mill, which is undesirable and can contaminate nearby streams, rivers, and land. In addition to serious environmental problems, including acidification, eutrophication, biodiversity loss, and climate change, POME has negative environmental effects, such as contaminating aquatic and terrestrial ecosystems (Sabiani *et al.*, 2023). In the oil wastewater cleanup process, the microorganisms that produce the lipase are typically employed (Enerijiofi *et al.*, 2024). If microorganisms used have an enzymatic profile, POME can undergo a more effective bioremediation process (Ganapathy *et al.*, 2019).

Although several microbial species have been found to remediate POME, little is known about the ability of environmental consortia, either native aerobic microbial enrichments or microbial consortia from highly polluted wastes, to remediate these wastewaters. However, the use of native microorganisms for POME remediation could improve their adaptability, survival, and capacity to degrade effluents with high levels of suspended organic solids, oil and grease, and elevated chemical and biochemical oxygen demand (Agualimpia *et al.*, 2016; Al-Kanany *et al.*, 2023).

The environmental challenges posed by POME have led to an intensive and integrated search for an eco-friendly alternative technique for the remediation of its pollutants. Microorganisms, including bacteria, molds, yeasts, and fungi, can completely degrade oil-based wastewater (Ganapathy *et al.*, 2019; Ndekhedehe *et al.*, 2023). Considering POME as the most environmentally harmful, the growing global consumption of palm oil therefore calls for an immediate response to reduce the pollution generated during its production. POME adversely affects the qualities of soil and water and has significant concentrations of contaminants like oil and grease. The pH of the soil changes through the release of POME into it, and this has an impact on the availability of nutrients for plants

(Olufunmilayo *et al*., 2023). POME also alters soil characteristics, including odor, color, and texture, causing pore waterlogging and subsequent vegetation death, ultimately leaving the environment bare.

Currently, POME and other oil processing waste treatments primarily use a single microbial species. However, a single organism can find it difficult to metabolize all the contaminating components to permissible discharge levels because most effluents have a variety of properties. Although single microbial species are still being investigated, mixed cultures offer several advantages in biodegradation research, including greater tolerance to environmental perturbations such as fluctuations in nutrient availability, pH, temperature, and pollutant concentrations (Patowary et al., 2023). It is of paramount importance to also note that microorganisms play a critical role in the natural attenuation and bioremediation of contaminated soils. Numerous studies have reported their ability to degrade contaminants and restore polluted environments. For example, Popoola and Olanbiwoninu (2019) demonstrated the potential of indigenous microorganisms to degrade Bonny crude oil in both pilot-scale field studies and controlled soil-contamination experiments. Several other studies have explored the microbial remediation of diverse soil contaminants, including heavy metals, petroleum hydrocarbons, and agrochemical residues (Yu *et al*., 2024; Li *et al*., 2025; Han *et al*., 2025). These findings underscore the feasibility of employing microbial communities as sustainable and cost-effective tools for restoring polluted soils. However, relatively few studies have focused specifically on the microbial remediation of palm oil mill effluent (POME)-contaminated soils, despite the significant ecological impact of POME discharge on soil health and productivity. It is important to investigate the potential of indigenous microorganisms, particularly *P. fluorescens*, for the bioremediation of POME-contaminated environments. This study, therefore, aims to evaluate the degradative capability of molecularly identified *P. fluorescens* on palm oil-contaminated soil.

MATERIALS AND METHODS

Sample collection and preparation

The palm-oil-contaminated soil was aseptically collected from Fiditi Oil Mill Centre, Oyo State, Nigeria, and uncontaminated soil samples were collected aseptically from the front of the Faculty of Natural Sciences at Ajayi Crowther University, Oyo State,

Nigeria. The palm oil was purchased from Ajegunle Market, Oyo, Oyo State, Nigeria. The soil samples were weighed to 250 g each into 18 mm diameter bowls. For the purposely contaminated samples, 20 mL of the palm oil was thoroughly mixed with 250 g of the soil sample for each of the 18 mm diameter bowls.

Inoculum Preparation and Addition

The isolate (*P. fluorescens*) (Isolate A) was used for the bioremediation experiment. The isolate was obtained from the Microbiology Laboratory, Ajayi Crowther University, Oyo State. The isolate was previously subjected to standard morphological and biochemical tests for its identification. The isolate was subsequently inoculated into nutrient broth and incubated for 24 h; thereafter, the cell count was determined using a hemocytometer (Marienfeld Superior, Germany) and standardized to obtain an inoculum size of 2×10^7 per mL. One milliliter (1 mL) of the isolate was dispersed in 9 mL of sterile distilled water and added to the soil in the different treatment bowls. The inoculated soil was then thoroughly mixed to ensure uniform distribution of the added microbial cells (Onajobi *et al.*, 2020).

Tilling

Soils with the "mixing" treatment option were tilled twice a week throughout the 12-week experimental study to improve soil aeration and enhance biodegradation. The soil without "mixing" was left undisturbed in the bowls throughout the study period.

Physico-chemical Analysis

The physico-chemical properties of the collected soil samples were determined for the following parameters using the procedure in the method of soil analysis (AOAC, 1980).

i. pH in Water

The soil samples were air-dried, and 10 g of each sample was placed in a beaker. The suspension was stirred several times over a 30-min interval, and the pH of the soil in each beaker was thereafter measured using the glass electrode of a pH meter.

ii. Moisture content (%)

The soil sample was air-dried for three days; thereafter, 50 g of the soil was placed in a pre-weighed aluminum tray. The aluminum tray containing the soil sample was placed in an oven and dried at 110 °C for 48 h. The tray and oven-dried soil were thereafter kept

in a desiccator for 1 h to cool. The weight of the tray and the oven-dried soil was then taken. The following formula was used to calculate the water activity in the soil.

$$\textbf{Moisture content} = \frac{Weight\ of\ soil\ before\ oven-drying}{Weight\ of\ oven-dried\ soil} \times 100\ \%$$

iii. Percentage of Organic Carbon:

The soil sample was ground to pass through a 60 mm mesh sieve, and 1 g of the sieved sample was measured in duplicates into two 250 mL conical flasks. 10 mL of 1N $K_2Cr_2O_7$ solution was pipetted into each flask and swirled gently to disperse the soil. 20 mL of concentrated H_2SO_4 was promptly added directly to the suspension and gently swirled immediately until the soil and the reagents had mixed. It was thereafter shaken vigorously for 60 s. The flask was rotated again and allowed to stand on the bench for 30 min. 100 mL of distilled water was then added, followed by 3–4 drops of ferroin indicator. The mixture was titrated with 0.5 N $FeSO_4$ solution using a burette. Greenish cast coloration in the solution, which changed to dark green, marked the end point of the titration.

The $FeSO_4$ solution was then added drop by drop until the color changed rapidly from blue to red. The blank titration (without soil) was carried out in the same manner to standardize the dichromate. The percentage of organic carbon in the soil sample was calculated as follows:

$$\textbf{Percentage of Organic Carbon} = \frac{me.K_2Cr_2O_7 = me.FeSO_4 \times 0.003}{Weight\ of\ oven-dried\ soils} \times 100\ (F)$$

Correction factor, F = 1.33

[Where meq. = Normality of solution × mL of solution used]

iv. Total Nitrogen

Five grams of an air-dried soil sample were ground and transferred to an 11 cm^3 Whatman No. 2 filter paper, wrapped, and dropped into a 500 mL Kjedahl flask. One heaped teaspoon (~11 g) of the digestion mixture was added to the flask through a long, wide, stern funnel; 25 mL of concentrated H_2SO_4 was added and swirled gently until the sample and acid were thoroughly mixed. The flask was then placed in the Kjeldahl digestion apparatus, and the fume aspirator was turned on. The mixture was heated at low temperatures until the organic matter was destroyed, as evidenced by the light grey or straw-colored mixture. The heat was turned off, the flask was then removed, and capped immediately. The whole unit was cooled until distilled water could be added without an

explosive result. 250 mL of distilled water was carefully added and mixed thoroughly. While holding the flask at a 45° angle, 75 mL of 40% NaOH was carefully added down the inner wall of the flask, allowing it to flow to the bottom without mixing. Three pieces of mossy zinc (Zn) were added, and the flask was attached immediately to the distillation unit at the receiving end, with a 500 mL flask containing 25 mL of 4 % boric acid (plus indicator) and 250 mL of water. The Kjeldahl flask was gently swirled to mix the contents at low heat.

About 200 mL of the mixture was collected in the receiving flask. The distillate was then titrated with a standard 1 M H_2SO_4 until the blue color disappeared. The endpoint was indicated as the solution turns pink. The volume of the acid required to titrate the blank (set up as a parallel) was subtracted from the amount used to titrate the sample. This gave the amount of nitrogen in the sample.

v. Available Phosphorus:

Five grams of the soil samples and a scoop of refined charcoal were placed in a 250 mL conical flask. 100 mL of the extracted solution containing 0.5 M $NaHCO_3$, adjusted to pH 8.5 with 0.1 N NaOH, was added and shaken for 30 min. The soil suspension was then filtered through a No. 40 filter paper, and 5 mL of the filtrate was pipetted into a 25 mL conical flask. 5 mL of 0.5 M ammonium molybdate solution was slowly added. The flask was shaken gently to mix the contents, and the neck of the flask was subsequently washed down, diluting the contents simultaneously with 22 mL of distilled water. 0.1 mL of dilute $SnCl_2$ solution was added and mixed. The transmittance of the solution was measured in the colorimeter at 660 nm, 10 min after adding the $SnCl_2$ solution, considering the value of available phosphorus (P) in the soil.

vi. Exchangeable Cations (Na and Mg)

10 g of the soil sample was weighed into a 250 mL conical flask. 1 mL of 1 N ammonium acetate was added, and the flask was stoppered. The suspension was intermittently agitated by manual shaking for 30 min, after which it was filtered through Whatman No. 1 filter paper. The first 10–20 mL of the obtained filtrate was discarded, and then 25 mL of the suspension was collected in a 50 mL conical flask. A flame photometer was used to determine the concentrations of Na and Mg cations in ppm, present in the soil sample. This was calculated as follows:

$$\textbf{ppm cation in soil} = \frac{ppm\ cation\ in\ solution \times vol.\ of\ extractant}{Weight\ of\ soil}\ (\times\ any\ further\ dil)$$

$$\textbf{mg/100g of soil} = \frac{ppm\ cation\ in\ soil}{10 \times mg\ wt.\ of\ cation}$$

Finally, the soil color was merely determined visually.

Bioremediation Setup and Treatment

The bioremediation setup and design are shown in Table 1 and Figure 1, respectively. Soil samples were taken in duplicates bi–weekly for 12 weeks from each bowl (18 mm diameter) of each treatment option by scooping the soil at the top, middle, and bottom with a sterile spoon, ensuring that the sample taken was a true representation of the treated soil. Soil sterilization of both polluted and unpolluted soil samples was sterilized at 121 °C for 3 consecutive days to eliminate all viable microorganisms present. This was done to ensure that only the inoculated bacterial isolate degrades the contaminants present in the soil. The biodegradation process was determined using the following methods:

i. Total Viable Count (Enumeration)

The total viable microbial count of the soil sample was determined over 12 weeks to enumerate the microorganisms present in the polluted soil based on their growth and metabolic activity. The pour plate technique was used, incubation at room temperature for 24 – 48 h. Colonies that developed were counted and recorded from the 2nd to the 12th week (Popoola *et al*., 2022; Onajobi *et al*., 2023).

ii. ***Spectrophotometric Analysis***

The residual oil present in each soil during the bioremediation experiment was determined according to the method highlighted by Cheesebrough (2006). 5 g of each soil sample was extracted with 10 mL n-Hexane for residual oil and allowed to stand for a few minutes. The optical density of the supernatant containing the extracted oil was determined with a UV/VIS spectrophotometer at 420 nm.

iii. Gravimetric Analysis

The modified method of Cheesebrough (2006) was used to determine the residual oil present in the soil during the bioremediation experiment. The residual oil present in the

soil after week 4 of bio-treatment was extracted as described above. The n-hexane was used as the extracting solvent at 50 °C, the residual oil obtained was then quantified in grams.

Molecular Characterization of Isolated Bacteria (DNA Extraction Procedure using the Zymo Kit)

Molecular characterization of isolated bacteria, focusing on DNA extraction, amplification, sequencing, and phylogenetic analysis, was conducted.

i. DNA Extraction and DNA Amplification (PCR)

Bacterial template DNA was extracted at the International Institute of Tropical Agriculture (IITA) in Ibadan using the Zymo Kit. The extraction was carried out by lysing the bacterial cells, purifying DNA, and eluting it for downstream applications. The extracted DNA underwent polymerase chain reaction (PCR) amplification. PCR amplification was performed in a 25 μL reaction mixture containing 1× PCR buffer (Thermo Fisher Scientific, USA), 2.0 mM $MgCl_2$, 0.2 mM of each dNTP, 0.5 μM of universal bacterial primers 27F (5'-AGAGTTTGATCMTGGCTCAG-3'), and 1525R (5'-AAGGAGGTGATCCAGCC-3'), 1 U of Taq DNA polymerase (Thermo Fisher Scientific, USA), and approximately 50 ng of template DNA (Ilesanmi *et al.*, 2020). PCR cycling was carried out in a Veriti 96-Well Thermal Cycler (Applied Biosystems, USA) with the following conditions: initial denaturation at 95 °C for 3 min, followed by 30 cycles of denaturation at 95 °C for 30 s, annealing at 55 °C for 30 s, and extension at 72 °C for 1 min, with a final elongation step at 72 °C for 10 min.

Amplified products were analyzed by electrophoresis on a 1.5% (w/v) agarose gel (Invitrogen UltraPure™ Agarose) prepared in 1× TAE buffer, stained with ethidium bromide (0.5 μg/mL), and visualized under UV illumination using a Gel Doc XR+ System (Bio-Rad, USA).

ii. **PCR Product Purification and DNA Sequencing**

PCR products were purified using ethanol precipitation. Ethanol was added to the PCR product, followed by centrifugation, washing with ethanol, and air drying. Purified amplicons were reconstituted in water and checked on agarose gel. Purified PCR products were sequenced at Inqaba Biotechnology Industrial (Pty) Ltd, Pretoria, South Africa, using the dideoxy chain termination method. Sequencing was performed on an ABI PRISM® 3500 XL DNA Sequencer (Ilesanmi *et al.*, 2020).

iii. Sequence Analysis and BLAST search analysis of 16S rRNA gene sequence

The 16S rRNA gene sequence was analyzed using the Basic Local Alignment Search Tool (BLAST) from the National Center for Biotechnology Information (NCBI), employing default parameters for homology identification. The hypervariable regions, specifically V3–V4 (positions ~341–806), of the 16S rRNA gene were sequenced for the molecular identification of the isolate.

iv. Molecular Phylogenetic Analysis

Molecular Evolutionary Genetics Analysis (MEGA) was used to generate a phylogenetic tree based on 16S rRNA gene sequences. The Maximum Likelihood method, based on the Tamura-Nei model, was employed to infer the evolutionary history of isolates. The final dataset comprised 511 positions. MEGA was utilized for evolutionary analyses and tree construction (Tamura *et al.* 2021).

Statistical Analysis

Data were expressed as mean ± standard error of the mean (SEM). One-way analysis of variance (ANOVA) was performed to assess differences among treatments, and significant differences between group means were determined using Duncan's Multiple Range Test (DMRT). A probability value of $p < 0.05$ was considered statistically significant.

RESULTS AND DISCUSSION

Assessment of physico-chemical alterations in palm oil mill effluent-contaminated soil and the effect of bioremediation

Long-term pollution may be the cause of the distinctive black coloration seen in the soil affected by POME. The physical and chemical characteristics of the soil have been significantly impacted by the ongoing exposure to waste discharge at this location, which has historically been utilized for the processing of palm oil. High concentrations of organic matter are suggested to be linked to black coloration, which is likely the result of organic residues and partial decomposition over time. This finding is corroborated by the data in Table 2, which shows that the polluted soil had higher values for physiochemical parameters, such as nitrogen, organic carbon, and phosphate, than the unpolluted soil. The increase in nutrient content demonstrates the long-lasting effects of improper palm oil

waste disposal practices on the ecosystem. This offers a clear indication of the level of contamination.

With reference to pH readings taken throughout the investigation, the polluted soil from the oil mill had a pH of 6.22, which is close to neutral. This result is consistent with research carried out by Okwute and Isu (2007), who found a higher value of 6.59. It's interesting to note that the uncontaminated soil had a pH of 6.5, which is very close to neutral. These results imply that both soils fall within a pH range that is suitable for plant growth and microbial activity. But by the end of the 12-week treatment period, the pH of the bioremediated and tilled soil sample had significantly changed, rising to 7.04.

The inoculation *of P. fluorescens*, a bacterium renowned for its effectiveness in biodegradation, is probably what caused this surge in microbial activity. Regular tilling also contributed to aeration, further enhancing microbial performance. The alkaline shift observed may have been the result of neutralization of acidic intermediates as biodegradation proceeded. The pattern corroborates the studies of Okwute and Isu (2007); Ohimain et al. (2012). Newly released POME typically has an acidic pH; however, pH levels gradually return to neutrality or even a modest alkalinity due to microbial activity and the timing. Notably, the measured pH levels remained below the effluent limitations set by the Federal Environmental Protection Agency (FEPA) (6–9), demonstrating bioremediation's ability to preserve environmentally acceptable soil conditions.

Nutrient analysis showed significant variations in nitrogen content across the soil samples. A moderate nitrogen level of 52.9 mg/kg was found in the biotreated and tilled contaminated soil, which was much higher than the 12.0 mg/kg found in the uncontaminated soil. These numbers imply a buildup of nitrogen in the polluted soils, possibly due to the organic content of palm oil waste, which contains nitrogen-rich residues from the oil extraction process. The total nitrogen and organic carbon levels were considerably increased in the contaminated soils compared to the unpolluted samples. The findings of other researchers who have recorded comparable increases in nutrient levels in soils affected by POME are consistent with this observation. The delayed decomposition of organic matter in saturated or anaerobic conditions, which are frequently present in POME-dumped sites, could account for the high organic carbon content. Such environments hinder rapid decomposition, causing the gradual accumulation of undecomposed organic material. This process can be further hindered in cooler or less

aerated soils, resulting in higher residual levels of organic carbon. This affects the fertility and microbial ecology of the soil in addition to changing its structure.

Analysis revealed a significantly greater concentration of total nitrogen and organic carbon in the oil mill-polluted soil relative to the unpolluted soil. This result aligns with previous studies on similar hydrocarbon-contaminated sites (Adesodun and Mbagwu, 2008; Okwute and Isu, 2007; Okwute *et al.*, 2015), suggesting a common impact of such pollution on soil chemical properties. The higher organic carbon value of the oil mill polluted soil can be attributed to the constituents of the raw and inadequate treatment of palm kernel effluent released into the soil. It is possible that a slow decomposition of organic matter in POME under water-saturated conditions, particularly when mean soil temperatures are low, contributed significantly to the higher organic carbon of the POME soil (Goveas *et al.*, 2024).

Phosphorus, an essential macronutrient for plant growth, was also significantly higher in contaminated soils. The highest phosphate level, 42.2 mg/kg, was recorded in the purposely contaminated and biotreated soil sample, followed by 39.5 mg/kg in the untreated contaminated control. In contrast, the uncontaminated soil had a substantially lower phosphate concentration of 16.2 mg/kg, which supports the findings of Zulkhifili *et al.* (2023). Substantial evidence indicates that phosphorus is the primary element regulating carbon and nitrogen immobilization. The increase in available phosphorus in the palm oil polluted soil suggests high absorption in the soil or precipitation of phosphate (Okwute and Isu, 2007). This may be due to the gradual biodegradation of the oil mill polluted soil, which leads to a delayed effect on the soil. The results could also imply that phosphorus availability rises with degradation, possibly due to mineralization or the release of phosphate molecules from decaying organic matter. High absorption capacity or precipitation processes within the soil matrix during the restoration of organic-rich polluted settings could be the cause of the increase in phosphorus (Nwachukwu *et al.*, 2018).

Another critical parameter examined in this study is the soil's cation exchange capacity (CEC), particularly with respect to sodium and magnesium levels. The data indicate significantly higher CEC values in the polluted soil than in the unpolluted samples. CEC is an essential indicator of soil fertility, which refers to the soil's ability to retain and exchange positively charged ions (cations) such as calcium, magnesium, potassium, and sodium, neutralizing negative charges in the soil (Tugiman *et al.*, 2024). Soils with high CEC

generally have greater capacity to hold nutrients and improved fertility. In the context of palm oil pollution, increased CEC may result from the abundance of organic residues and the high microbial activity promoted by the presence of degradable substrates. The study's findings are consistent with previous research, which documented increased CEC near sources of effluent discharge (Okwute and Isu, 2007). This enhancement in CEC not only signifies better nutrient retention but also indicates the soil's potential to recover its agricultural value through effective bioremediation.

Moisture content (%), which is the amount of water available for biological and chemical reactions, was also affected by pollution and treatment processes. Moisture content (%) represents the availability of moisture in the soil, a crucial factor for microbial growth and the enzymatic process. After 12 weeks of treatment, the bioremediated and tilled soil sample showed a much lower moisture content (5.77%) compared to the untreated contaminated control (28.4%). The decline in moisture availability suggests that microbial communities in the bioremediated soil actively utilized water for metabolic and degradation activities, since water availability is a key regulator of ecosystem functioning, directly controlling soil microbial activity (Engelhardt, 2018).

Periodic tilling may have enhanced evaporation and aeration, which could account for the decline. Given that water is a key regulator of microbial function and ecosystem productivity, the observed trend is consistent with ecological principles. Noteworthy is the fact that as moisture rises, microbial deterioration proceeds because metabolic activities use water. Therefore, increased biological activity may be the cause of the treated soil's decreased water activity, demonstrating the efficacy of the bioremediation technique used.

Heterotrophic Count of Soil Samples

The total viable heterotrophic counts in all soil samples (with different treatments) over 12 weeks are presented in Table 3. The microbial counts followed a similar pattern for almost all the samples, as shown in the Table, the counts decreased over the 12 Weeks of bioremediation. For instance, sterile oil mill soil + *P. fluorescens* with tilling (SCPT), was 11.500 ± 1.12 $\log_{10}$ CFU/g in Week 2, decreased to 9.350 ± 1.02 $\log_{10}$ CFU/g by Week 12, while sterile purposely contaminated soil + *P. fluorescens* **(**SPP) had a count of 11.239±1.72 $\log_{10}$ CFU/g in Week 2, by the 12th Week the count was 8.000±1.51 $\log_{10}$ CFU/g. Although oil mill soil + *P. fluorescens* and oil mill soil + *P. fluorescens* with tilling (CP and CPT; with a

standard deviation of 0.35 and 0.88, respectively) had a close range of microbial counts through the period of bioremediation, with CPT having 11.628±0.67 $\log_{10}$ CFU/g in Week 2 and 10.602±0.35 $\log_{10}$ CFU/g by Week 12.

It is worth noting, however, that the values for the sterile oil mill soil + *P. fluorescens* with tilling (SCPT) sample are consistently higher than those of the sterile oil mill soil + *P. fluorescens* (SCP) sample, suggesting that tilling may have contributed to a higher microbial count. The standard deviation for the SCPT row is 1.08, which is slightly lower than that of the SCP row, indicating less variability in the measurements. SCP, purposely contaminated soil + *P. fluorescens* **(**PCS), and purposely contaminated soil + *P. fluorescens* with tilling (PPT) were all significantly lower by the 12th week at $p < 0.05$.

In this study, the total viable bacterial counts in the sterile and non-sterile samples from the oil mill for both tilled and untilled conditions generally increased from day 0 to the 4th week and then 6th week, and there was an eventual decline in the cell number at the 12th week. The increase in the first four weeks indicated that the organism (*P. fluorescens*) was able to utilize the substrate present in the palm oil polluted soil; however, the reduction as the week progressed could be a result of the continued degradation of palm oil in the soil. The decrease in the number of organisms could be attributed to nutrient limitation over time, and the bacterial load of the palm oil polluted soil was higher than that of the non-polluted soil. This may be attributed to the higher organic matter content in the POME and a more favorable pH, as also affirmed by Olufunmilayo (2023).

Spectrophotometric Analysis of Samples

The results of a spectrophotometric analysis conducted on soil samples over 12 weeks are shown in Table 4. The analyses aimed to assess the presence of a specific analyte potentially related to hydrocarbon contamination in various soil samples. The uncontaminated soil (US) consistently showed no detectable levels of the analyte throughout the study. The fluctuations in analyte levels over time and across different sample types suggest that various factors, such as the presence of isolates, tilling, and the initial level of contamination, may have influenced the degradation or transformation of the target contaminant in the soil samples.

At day 0, US and the oil mill contaminated soil (CS) showed non-zero absorbance values, indicating the presence of the analyte in the contaminated soil sample. The

purposely contaminated soil samples (PCS) also exhibited a significant absorbance value at day 0. As the experiment progressed, the absorbance values for most of the treated soil samples increased at Week 4, suggesting an initial increase in the concentration of the analyte. This could be due to microbial degradation of the oil present in the soil, as well as metabolic release. This is evident in the reduced quantity of residual oil obtained in the gravimetric analysis in the 4th week (Table 5). The degradation of the vegetable oil into fatty acid and other simple inorganic chemical compounds may also be responsible for the reduction in the turbidity of the solvent by the 8th week (Mahmoud *et al.*, 2023).

However, by Week 8 and Week 12, the absorbance values for most of the treated soil samples decreased, indicating a reduction in the concentration of the analyte over time. This supports the findings of Zulkhifli *et al.* (2023), suggesting that the various treatments applied to the contaminated soil samples, such as the addition of bacterial isolates and tilling, potentially aided in the remediation or degradation of the contaminant present in the soil.

The data suggest that the treatments were effective in reducing the concentration of the analyte over the 12-week experiment. It is noteworthy that the interpretation of the results may require additional information about the specific contaminant being analyzed, the nature of the bacterial isolates used, and the experimental conditions under which the analysis was performed. However, the overall trend observed in the data suggests that the applied treatments had a positive impact on the remediation of the contaminated soil samples over time (Onajobi *et al.*, 2023).

Gravimetric Analysis of Soil Samples

The residual oil present in each soil (remediation bowl) was extracted using n-hexane during the remediation process. Table 5 presents the different quantities of residual oil from each bowl, measured in grams. The gravimetric analysis of soil samples from day 0 to Week 12 provides valuable insights into the dynamics of soil contaminants and the potential effects of various treatments. At the outset, it is of great importance to note that samples, such as the US, had no recorded values throughout the 12 weeks. This serves as a baseline or control for comparison with the other soil samples that underwent various treatments. One notable observation is the relatively high initial weight of the purposely contaminated soil plus *P. fluorescens* (PCS) sample, 0.130 g at day 0. This value gradually

decreased over time, reaching 0.080 g by the 12th Week. This reduction in weight could be attributed to the degradation or removal of the oil contaminant from the soil, likely due to the introduction of the isolate or other bioremediation processes.

Interestingly, SCP and the sterile purposely contaminated soil with the isolate and tilling (SPPT) exhibited residual oil weight increase from Week 4 to Week 8, before decreasing by Week 12. This suggests that the initial stages of bioremediation may have involved the growth or accumulation of components such as microbial biomass or metabolic byproducts, resulting in an initial weight gain (Popoola *et al*., 2022).

However, the subsequent decrease in weight by Week 12 could indicate the successful degradation or removal of the oil contaminant from the soil. The oil mill soil samples (CS and CP) displayed relatively low weights of residual oil throughout the experimental period, with some fluctuations. This could be due to varying levels of degradation in these samples. The introduction of tilling, as seen in the SCPT, SPPT, CPT, and PPT samples, appears to have had an impact on the soil weights. While some samples exhibited either increases or decreases in residual oil weight, the overall pattern suggests that tilling influenced the dynamics of the bioremediation process, possibly by enhancing aeration, nutrient availability, and microbial activity. This shows that *P. fluorescens* can be employed in the bioremediation of an oil mill polluted site with the use of tilling, which also "corroborates" the work of Fanaei *et al.* (2020).

This release could be due to the acclimatization of the inoculated organism, which degrades most complex products into alcohol and acids. It was observed that at the end of the 12th week, there was a decrease in both the turbidity and the residual oil weight in the samples, which indicated that the organism helped to break down the POME into less toxic forms, which is consistent with the work of Okwute and Isu (2007) and Nwuche *et al.* (2014).

It is worth noting that gravimetric analysis alone does not provide a complete picture of the bioremediation process. Additional analyses, such as chemical characterization of the contaminants, microbial population studies, and plant growth assessments, would be necessary to gain a more comprehensive understanding of the efficacy of the treatments and the mechanisms involved. The observed patterns suggest the potential impact of treatments like isolate introduction, tilling, and the presence of contaminants on the dynamics of soil contaminants and bioremediation processes. Further

analyses and interpretation in conjunction with other data would be necessary to draw more comprehensive conclusions and develop effective bioremediation strategies for contaminated soils.

Molecular Characterization, sequencing, and evolutionary relationships of taxa

The bacterial isolate was molecularly characterized using 16S rRNA gene sequencing, and the resulting sequences were compared with those in the National Center for Biotechnology Information (NCBI) database using the Basic Local Alignment Search Tool (BLAST). The regions of the 16S rRNA gene that were sequenced are the hypervariable regions, specifically V3–V4 (positions ~341–806), because they contain enough variation to distinguish between genera (and sometimes species), while still being flanked by conserved regions that allow for universal primer binding, this was also in agreement with the study by Hiergeist *et al.* (2023), who also sequenced around similar region. The result provided critical insights into the identity of the isolated bacteria, the genetic similarity to known strains, and their evolutionary relationships.

NCBI BLAST was used to identify and analyze the sequences of the bacterial isolate. Table 6, which contains the organism name, strain identities, percentage identity scores, and the accession number from the NCBI database, provides a summary of the comprehensive results. *P. fluorescens*, strain OYB-2, was successfully identified as Isolate A and utilized in the bioremediation experiment. A remarkable 100.00% identity was found in the BLAST output with the reference sequence, which had the accession number MN607218.1.

The strength and reliability of 16S rRNA gene sequencing as a molecular identification tool were evident in the results obtained for the bacterial isolates. Isolate A showed a 100% sequence identity with a well-characterized *P. fluorescens* strain in the NCBI database, confirming its genetic stability and close similarity to previously reported strains. This perfect match indicates that the isolate belongs to a highly conserved lineage, with no detectable genetic deviation from its reference sequence.

To better understand the evolutionary relationships of this isolate, a phylogenetic tree was constructed using the Neighbour-Joining (NJ) method, as described by Tamura *et al.* (2021) (Figure 2). The tree topology revealed that both isolates clustered within the *P. fluorescens* clade, with branch lengths reflecting evolutionary distances calculated via the

Poisson correction method. These distances represent the number of amino acid substitutions per site, thereby providing a quantitative measure of genetic divergence among sequences (Chato et al., 2022). The robustness of the clustering was confirmed by high bootstrap values at the internal nodes, indicating strong confidence in the branching pattern. Such phylogenetic visualization is instrumental in elucidating the evolutionary history and genetic relatedness of the isolates to their nearest ancestors.

Collectively, the results confirm the identity of the isolate as *Pseudomonas fluorescens* and highlight notable differences in genetic similarity. Isolate A represents a genetically stable strain. These findings further validate the use of 16S rRNA gene sequencing as a reliable tool for bacterial identification and provide insights into the evolutionary dynamics of bacterial populations involved in the bioremediation of palm oil mill effluent–contaminated soils.

Table 1: Soil samples and treatment employed

S/N	SOIL SAMPLES AND TREATMENT	CODES
	Uncontaminated soil	US
1.	Oil mill soil	CS
2.	Oil mill soil + P. fluorescens	CP
3.	Oil mill soil + P. fluorescens with tilling	CPT
4.	Sterile oil mill soil + P. fluorescens	SCP
5.	Sterile oil mill soil + P. fluorescens with tilling	SCPT
6.	Purposely contaminated soil	PC
7.	Purposely contaminated soil + P. fluorescens	PCS
8.	Purposely contaminated soil + P. fluorescens with tilling	PPT
9.	Sterile purposely contaminated soil + P. fluorescens	SPP
10.	Sterile purposely contaminated soil + P. fluorescens with tilling	SPPT

Table 2: The Physico-chemical analysis of soil samples

S\N	Parameters	Purposely Contaminated Soil (Control)	Purposely Contaminated Soil + Organism + Tilling (week 12)	Uncontaminated Soil (Control)	Contaminated Soil (Control)
1	pH	6.98 ± 0.087^{a}	7.04 ± 0.126^{a}	6.50 ± 0.034^{b}	6.22 ± 0.216^{b}
2	Moisture content (%)	28.4 ± 1.08^{a}	5.77 ± 1.71^{c}	12.2 ± 1.65^{b}	3.22 ± 1.42^{c}
3	Organic carbon (%)	6.85 ± 4.80^{a}	6.21 ± 2.40^{a}	1.41 ± 0.12^{c}	4.17 ± 0.24^{b}
4	Nitrogen (mg/kg)	83.7 ± 4.21^{a}	52.9 ± 5.12^{b}	12.0 ± 4.87^{c}	66.4 ± 4.02^{ab}
5	Phosphate	39.5 ± 2.82^{ab}	42.2 ± 3.12^{a}	16.20 ± 5.12^{c}	32.5 ± 5.21^{b}

S\N	Parameters	Purposely Contaminated Soil (Control)	Purposely Contaminated Soil + Organism + Tilling (week 12)	Uncontaminated Soil (Control)	Contaminated Soil (Control)
	(mg/kg)				
6	Sodium (mg/kg)	126.0±12.23^{a}	36.8±5.54^{c}	120.0±9.81^{a}	124.0±10.87^{a}
7	Magnesium (mg/kg)	12.4±0.13^{c}	16.9±0.26^{b}	21.50±0.32^{a}	15.3±0.42^{b}
8	Color	Blackish	Blackish	Dark-brown	Blackish

Key: SCP: Sterile oil mill soil + isolate; SCPT: Sterile oil mill soil + isolate with tilling; CPT: Oil mill soil + isolate with tilling; CP: Oil mill soil + isolate; SPP: Sterile purposely contaminated soil + isolate; SPPT: Sterile purposely contaminated soil + isolate with tilling; PCS: Purposely contaminated soil + isolate; PPT: Purposely contaminated soil + isolate with tilling; Data are presented as mean ± standard error of the mean (SEM). Means followed by different superscript letters within the same column (or row) are significantly different according to Duncan's Multiple Range Test (DMRT) at $p < 0.05$. SD: Standard Deviation.

Table 3: Total viable bacterial counts in soil samples over 12 weeks (log_{10}CFU/g)

Sample	Week 2	Week 4	Week 6	Week 8	Week 10	Week 12	SD
SCP	11.150±2.12^{a}	11.451±2.42^{a}	9.801±0.77^{b}	7.650±1.37^{c}	7.128±1.89^{d}	6.952±2.07^{d}	1.86
SCPT	11.500±1.12^{a}	11.923±1.55^{a}	10.801±0.42^{b}	9.321±1.05^{b}	9.340±1.03^{c}	9.350±1.02^{c}	1.08
CP	11.302±0.58^{a}	10.861±0.14^{b}	10.801±0.08^{b}	10.772±0.05^{a}	10.362±0.35^{b}	10.224±0.49^{b}	0.35
CPT	11.628±0.67^{a}	11.239±0.28^{b}	10.939±0.01^{b}	10.811±0.14^{a}	10.494±0.45^{b}	10.602±0.35^{b}	0.88
SPP	11.239±1.72^{a}	11.588±2.07^{a}	9.278±0.23^{bc}	8.651±0.86^{bc}	8.327±1.18^{c}	8.000±1.51^{c}	1.40
SPPT	11.573±1.05^{a}	11.690±1.17^{a}	9.418±1.09^{bc}	10.278±0.23^{ab}	11.088±0.57^{a}	9.040±1.47^{c}	1.02
PCS	11.150±1.17^{a}	11.451±1.47^{a}	11.907±1.93^{a}	10.128±0.15^{ab}	8.253±1.72^{c}	6.952±3.02^{d}	1.79
PPT	11.255±0.57^{a}	11.750±1.07^{a}	12.600±1.92^{a}	11.000±0.32^{a}	10.234±0.44^{b}	7.240±3.40^{d}	1.69

Key: SCP: Sterile oil mill soil + isolate; SCPT: Sterile oil mill soil + isolate with tilling; CPT: Oil mill soil + isolate with tilling; CP: Oil mill soil + isolate; SPP: Sterile purposely contaminated soil + isolate; SPPT: Sterile purposely contaminated soil + isolate with tilling; PCS: Purposely contaminated soil + isolate; PPT: Purposely contaminated soil + isolate with tilling; Data are presented as mean ± standard error of the mean (SEM). Means followed by different superscript letters within the same column (or row) are significantly different according to Duncan's Multiple Range Test (DMRT) at $p < 0.05$. SD: Standard Deviation.

Table 4: Spectrophotometric analysis of residual oil in soil samples from Day 0 to the 12th week (AU)

S\N	Samples	Day 0	Week 4	Week 8	Week 12
1	US	0.000	0.000	0.000	0.000
2	CS	0.089	0.360	0.247	0.085
3	PC	0.312	0.800	0.150	0.045
4	PCS	0.312	0.228	0.155	0.007
5	PPT	0.312	0.610	0.277	0.042
6	SPP	0.312	0.172	0.171	0.026
7	SPPT	0.312	0.260	0.165	0.019
8	CP	0.089	0.826	0.220	0.050
9	CPT	0.089	0.210	0.191	0.030
10	SCP	0.089	0.900	0.165	0.050
11	SCPT	0.089	0.210	0.191	0.030

Keys: US: Uncontaminated soil; CS: Oil mill soil; SCP: Sterile oil mill soil + isolate ; SPP: Sterile purposely contaminated soil + isolate; PC: Purposely contaminated soil; PCS: Purposely contaminated soil + isolate; CP: Oil mill soil + isolate; SCPT: Sterile oil mill soil + isolate with tilling; SPPT: Sterile purposely contaminated soil + isolate with tilling ; CPT: Oil mill soil + isolate with tilling; PPT: Purposely contaminated soil + isolate with tilling; CPT= contaminated soil + isolate + Tilling; Isolate = *Pseudomonas fluorescens.*

Table 5: Total recoverable residual oil of soil sample (g) from Day 0 to the 12th week in (g)

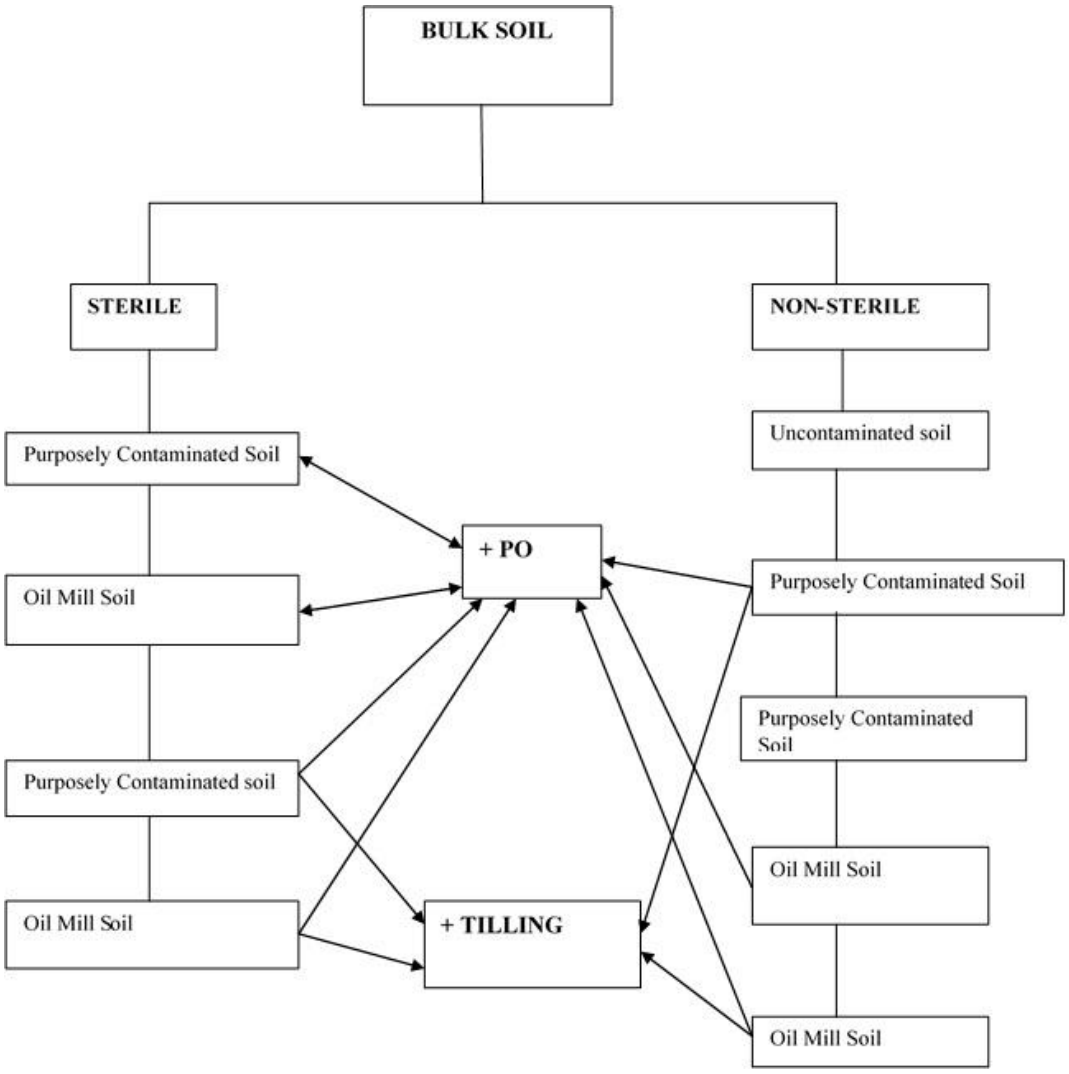
S/N	Sample	Day 0	Week 4	Week 8	Week 12
1	US	-	-	-	-
2	CS	0.020	0.010	0.030	0.020
3	PC	0.130	0.087	0.128	0.124
4	PCS	0.130	0.080	0.090	0.080
5	SCP	0.020	0.020	0.080	0.010
6	SPP	0.130	0.110	0.190	0.100
7	CP	0.020	0.010	0.050	0.000
8	SCPT	0.020	0.060	0.080	0.020
9	SPPT	0.130	0.070	0.170	0.100
10	CPT	0.020	0.020	0.080	0.010
11	PPT	0.130	0.070	0.050	0.070

Keys: US: Uncontaminated soil; CS: Oil mill soil; SCP: Sterile oil mill soil + isolate; SPP: Sterile purposely contaminated soil + isolate; PC: Purposely contaminated soil; PCS: Purposely contaminated soil + isolate; CP: Oil mill soil + isolate; SCPT: Sterile oil mill soil + isolate with tilling; SPPT: Sterile purposely contaminated soil + isolate with tilling; CPT: Oil mill soil + isolate with tilling; PPT: Purposely contaminated soil + isolate with tilling;

CPT= contaminated soil + isolate + Tilling; - Nil; g – gram; Isolate = *Pseudomonas fluorescens.*

Table 6: NCBI Sequence blasting of Bacterial isolate using 16s rRNA

Isolates code	Identified organism	Strain	Percentage identity (%)	Accession number
A	*P. fluorescens*	OYB-2	100.00%	MN607218.1



Where PO is *Pseudomonas fluorescens*

Figure 1: Experimental Design

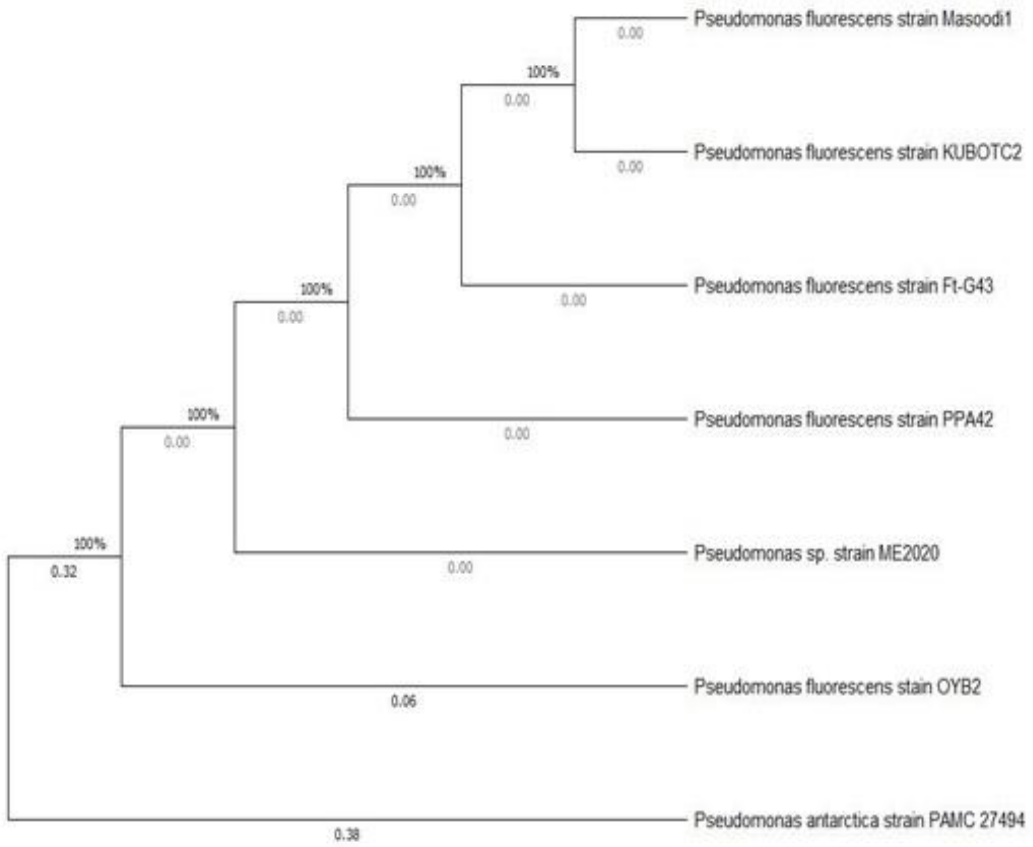


Figure 2: Phylogenetic tree of bacterial isolates constructed using Neighbor-Joining method (MEGA 11)

CONCLUSION

The study demonstrates the effectiveness of bioremediation in treating palm oil-contaminated soil using the bacterial species *P. fluorescens*. Significant remediation was achieved within 2-12 weeks, indicating the potential application in areas affected by palm oil pollution. The success of the bioremediation process is attributed to the balanced combination of microbial seeding and tilling/non-tilling techniques, which created favorable conditions for bacterial growth and efficient pollutant degradation. The ability of *P. fluorescens* (Isolate A) to effectively remediate palm oil-contaminated soil positions this bacterial species as a promising candidate for the development of microbial bioaugmentation products. These products could provide a targeted and efficient solution for treating palm oil pollution across various settings. Nevertheless, further research is necessary to elucidate the mechanisms underlying the remediation capabilities of *P.*

fluorescens and to optimize its application under diverse environmental conditions. The promising potential of *P. fluorescens* as an effective bioremediation agent for palm oil-contaminated soil warrants continued investigation. The development of microbial bioaugmentation products based on this bacterial species could provide a promising solution for addressing the growing concerns associated with palm oil pollution. Further research and development in this area could help establish sustainable and efficient bioremediation strategies aimed towards protecting both the environment and human health.

REFERENCES

Ahmed, M., Hashmi, T. M., Shafiq, A., Ashraf, H., Jain, H., Khanji, M. Y., Providência, R., Chahal, A. A., Rana, J. S., Farhan, M., Ahmed, R., Fudim, M., & Fonarow, G. C. (2025). Efficacy and safety of colchicine in patients with coronary artery disease: An updated meta-analysis of randomized controlled trials. *American Heart Journal Plus: Cardiology Research and Practice, 59*, Article 100610. https://doi.org/10.1016/j.ahjo.2025.100610

Ajoolabady, A., Pratico, D., Lin, L., Mantzoros, C. S., Bahijri, S., Tuomilehto, J., & Ren, J. (2024). Inflammation in atherosclerosis: Pathophysiology and mechanisms. *Cell Death & Disease, 15*(11), Article 817. https://doi.org/10.1038/s41419-024-07166-8

Baker, R. G., Hayden, M. S., & Ghosh, S. (2011). NF-κB, inflammation, and metabolic disease. *Cell Metabolism, 13*(1), 11–22. https://doi.org/10.1016/j.cmet.2010.12.008

Balsinde, J., Winstead, M. V., & Dennis, E. A. (2002). Phospholipase A2 regulation of arachidonic acid mobilization. *FEBS Letters, 531*(1), 2–6. https://doi.org/10.1016/S0014-5793(02)03413-0

Blake, G. J., & Ridker, P. M. (2000). Are statins anti-inflammatory? *Trials, 1*, Article 161. https://doi.org/10.1186/cvm-1-3-161

Chávez-Sánchez, L., Madrid-Miller, A., Chávez-Rueda, K., Legorreta-Haquet, M. V., Tesoro-Cruz, E., & Blanco-Favela, F. (2010). Activation of TLR2 and TLR4 by minimally modified low-density lipoprotein in human macrophages and monocytes triggers the inflammatory response. *Human Immunology, 71*(8), 737–744. https://doi.org/10.1016/j.humimm.2010.05.005

Cominacini, L., Fratta Pasini, A., Garbin, U., Davoli, A., Tosetti, M. L., Campagnola, M., Rigoni, A., Pastorino, A. M., Lo Cascio, V., & Sawamura, T. (2000). Oxidized low-density lipoprotein (ox-LDL) binding to ox-LDL receptor-1 in endothelial cells induces the activation of NF-κB through an increased production of intracellular reactive oxygen species. *Journal of Biological Chemistry, 275*(17), 12633–12638. https://doi.org/10.1074/jbc.275.17.12633

Cyr, A. R., Huckaby, L. V., Shiva, S. S., & Zuckerbraun, B. S. (2020). Nitric oxide and endothelial dysfunction. *Critical Care Clinics, 36*(2), 307–321. https://doi.org/10.1016/j.ccc.2019.12.009

Feng, B., Yao, P. M., Li, Y., Devlin, C. M., Zhang, D., Harding, H. P., Sweeney, M., Rong, J. X., Kuriakose, G., Fisher, E. A., Marks, A. R., Ron, D., & Tabas, I. (2003). The endoplasmic reticulum is the site of cholesterol-induced cytotoxicity in macrophages. *Nature Cell Biology, 5*(9), 781–792. https://doi.org/10.1038/ncb1035

Funk, C. D. (2001). Prostaglandins and leukotrienes: Advances in eicosanoid biology. *Science, 294*(5548), 1871–1875. https://doi.org/10.1126/science.294.5548.1871

Gimbrone, M. A., Jr., & García-Cardeña, G. (2016). Endothelial cell dysfunction and the pathobiology of atherosclerosis. *Circulation Research, 118*(4), 620–636. https://doi.org/10.1161/CIRCRESAHA.115.306301

Hansson, G. K., & Hermansson, A. (2011). The immune system in atherosclerosis. *Nature Immunology, 12*(3), 204–212. https://doi.org/10.1038/ni.2001

Hansson, G. K., Robertson, A.-K. L., & Söderberg-Nauclér, C. (2006). Inflammation and atherosclerosis. *Annual Review of Pathology: Mechanisms of Disease, 1*, 297–329. https://doi.org/10.1146/annurev.pathol.1.110304.100100

Harrington, R. A. (2017). Targeting inflammation in coronary artery disease. *New England Journal of Medicine, 377*(12), 1197–1198. https://doi.org/10.1056/NEJMe1709904

Huang, Y., Wang, Y., Wang, Y., Yi, S., Fan, Z., Sun, L., & Dou, G. (2014). Role of macrophage matrix metalloproteinase expression in plaque vulnerability. *International Journal of Molecular Medicine, 34*(2), 456–464. https://doi.org/10.3892/ijmm.2014.1646

Imazio, M. (2024). Colchicine for the treatment of the spectrum of atherosclerotic events: Clinical evidence. *Journal of Cardiovascular Medicine, 25*(9), 653–663. https://doi.org/10.2459/JCM.0000000000001647

Jiang, H., Zhou, Y., Nabavi, S. M., Sahebkar, A., Little, P. J., Xu, S., Weng, J., & Ge, J. (2022). Mechanisms of oxidized LDL-mediated endothelial dysfunction and its consequences for the development of atherosclerosis. *Frontiers in Cardiovascular Medicine, 9*, Article 925923. https://doi.org/10.3389/fcvm.2022.925923

Kawai, T., & Akira, S. (2007). Signaling to NF-κB by Toll-like receptors. *Trends in Molecular Medicine, 13*(11), 460–469. https://doi.org/10.1016/j.molmed.2007.09.002

Khan, M. S., Talha, K. M., Maqsood, M. H., Rymer, J. A., Borlaug, B. A., Docherty, K. F., Pandey, A., Kahles, F., Cikes, M., Lam, C. S. P., Ducharme, A., Voors, A. A., Hernandez, A. F., Lincoff, A. M., Petrie, M. C., Ridker, P. M., & Fudim, M. (2024). Interleukin-6 and cardiovascular events in healthy adults: MESA. *JACC: Advances, 3*(8), Article 101063. https://doi.org/10.1016/j.jacadv.2024.101063

Kong, P., Cui, Z.-Y., Huang, X.-F., Zhang, D.-D., Guo, R.-J., & Han, M. (2022). Inflammation and atherosclerosis: Signaling pathways and therapeutic intervention. *Signal Transduction and Targeted Therapy, 7*, Article 131. https://doi.org/10.1038/s41392-022-00955-7

Li, D., & Mehta, J. L. (2000). Upregulation of endothelial receptor for oxidized LDL (LOX-1) by oxidized LDL and implications in apoptosis of human coronary artery endothelial cells: Evidence from use of antisense LOX-1 mRNA and chemical inhibitors. *Arteriosclerosis, Thrombosis, and Vascular Biology, 20*(4), 1116–1122. https://doi.org/10.1161/01.ATV.20.4.1116

Li, L., Liu, S., Tan, J., Wei, L., Wu, D., Gao, S., Weng, Y., & Chen, J. (2022). Recent advance in treatment of atherosclerosis: Key targets and plaque-positioned delivery strategies. *Journal of Tissue Engineering, 13*, Article 20417314221088509. https://doi.org/10.1177/20417314221088509

Li, Y., Schwabe, R. F., DeVries-Seimon, T., Yao, P. M., Gerbod-Giannone, M.-C., Tall, A. R., Davis, R. J., Flavell, R., Brenner, D. A., & Tabas, I. (2005). Free cholesterol-loaded macrophages are an abundant source of tumor necrosis factor-alpha and interleukin-6: Model of NF-κB- and MAP kinase-dependent inflammation in advanced atherosclerosis. *Journal of Biological Chemistry, 280*(23), 21763–21772. https://doi.org/10.1074/jbc.M501759200

Libby, P. (2002). Inflammation in atherosclerosis. *Nature, 420*, 868–874. https://doi.org/10.1038/nature01323

Libby, P. (2021). Inflammation during the life cycle of the atherosclerotic plaque. *Cardiovascular Research, 117*(13), 2525–2536. https://doi.org/10.1093/cvr/cvab303

Libby, P. (2021). Inflammation in atherosclerosis: Transition from theory to practice. *Journal of the American College of Cardiology, 77*(12), 1560–1570. https://doi.org/10.1016/j.jacc.2021.01.032

Libby, P., Tabas, I., Fredman, G., & Fisher, E. A. (2014). Inflammation and its resolution as determinants of acute coronary syndromes. *Circulation Research, 114*(12), 1867–1879. https://doi.org/10.1161/CIRCRESAHA.114.302699

Lin, J., Kakkar, V., & Lu, X. (2014). Impact of MCP-1 in atherosclerosis. *Current Pharmaceutical Design, 20*(28), 4580–4588. https://doi.org/10.2174/1381612820666140522115801

Mehta, J. L., Sanada, N., Hu, C. P., Chen, J., Dandapat, A., Sugawara, F., Satoh, H., Inoue, K., Kawase, Y., Jishage, K.-I., Suzuki, H., Takeya, M., Schnackenberg, L., Beger, R., Hermonat, P. L., Thomas, M., & Sawamura, T. (2007). Deletion of LOX-1 reduces atherogenesis in LDLR knockout mice fed high-cholesterol diet. *Circulation Research, 100*(11), 1634–1642. https://doi.org/10.1161/CIRCRESAHA.107.149724

Mehta, N. N., deGoma, E., & Shapiro, M. D. (2024). IL-6 and cardiovascular risk: A narrative review. *Current Atherosclerosis Reports, 27*, Article 12. https://doi.org/10.1007/s11883-024-01259-7

Miller, Y. I., Choi, S.-H., Wiesner, P., Fang, L., Harkewicz, R., Hartvigsen, K., Boullier, A., Gonen, A., Diehl, C. J., Que, X., Montano, E., Shaw, P. X., Tsimikas, S., Binder, C. J., & Witztum, J. L. (2011). Oxidation-specific epitopes are danger-associated molecular patterns recognized by pattern recognition receptors of innate immunity. *Circulation Research, 108*(2), 235–248. https://doi.org/10.1161/CIRCRESAHA.110.223875

Nedkoff, L., Briffa, T., Zemedikun, D., Herrington, S., & Wright, F. L. (2023). Global trends in atherosclerotic cardiovascular disease. *Clinical Therapeutics, 45*(11), 1087–1091. https://doi.org/10.1016/j.clinthera.2023.09.020

Pirillo, A., Norata, G. D., & Catapano, A. L. (2013). LOX-1, OxLDL, and atherosclerosis. *Mediators of Inflammation, 2013*, Article 152786. https://doi.org/10.1155/2013/152786

Poston, R. N. (2019). Atherosclerosis: Integration of its pathogenesis as a self-perpetuating propagating inflammation: A review. *Cardiovascular Endocrinology and Metabolism, 8*(2), 51–61. https://doi.org/10.1097/XCE.0000000000000172

Poznyak, A. V., Nikiforov, N. G., Markin, A. M., Kashirskikh, D. A., Myasoedova, V. A., Gerasimova, E. V., & Orekhov, A. N. (2021). Overview of OxLDL and its impact on cardiovascular health: Focus on atherosclerosis. *Frontiers in Pharmacology, 11*, Article 613780. https://doi.org/10.3389/fphar.2020.613780

Rajendran, P., Rengarajan, T., Thangavel, J., Nishigaki, Y., Sakthisekaran, D., Sethi, G., & Nishigaki, I. (2013). The vascular endothelium and human diseases. *International Journal of Biological Sciences, 9*(10), 1057–1069. https://doi.org/10.7150/ijbs.7502

Ridker, P. M., Danielson, E., Fonseca, F. A. H., Genest, J., Gotto, A. M., Jr., Kastelein, J. J. P., Koenig, W., Libby, P., Lorenzatti, A. J., MacFadyen, J. G., Nordestgaard, B. G., Shepherd, J., Willerson, J. T., & Glynn, R. J. (2008). Rosuvastatin to prevent vascular events in men and women with elevated C-reactive protein. *New England Journal of Medicine, 359*(21), 2195–2207. https://doi.org/10.1056/NEJMoa0807646

Ridker, P. M., Devalaraja, M., Baeres, F. M. M., Engelmann, M. D. M., Hovingh, G. K., Ivkovic, M., Lo, L., Kling, D., Pergola, P., Raj, D., Libby, P., & Davidson, M. (2021). IL-6 inhibition with ziltivekimab in patients at high atherosclerotic risk (RESCUE): A double-blind, randomised, placebo-controlled, phase 2 trial. *The Lancet, 397*(10289), 2060–2069. https://doi.org/10.1016/S0140-6736(21)00520-1

Ridker, P. M., Everett, B. M., Thuren, T., MacFadyen, J. G., Chang, W. H., Ballantyne, C., Fonseca, F., Nicolau, J., Koenig, W., Anker, S. D., Kastelein, J. J. P., Cornel, J. H., Pais, P., Pella, D., Genest, J., Cifkova, R., Lorenzatti, A., Forster, T., Kobalava, Z., … Glynn, R. J. (2017). Antiinflammatory therapy with canakinumab for atherosclerotic disease. *New England Journal of Medicine, 377*(12), 1119–1131. https://doi.org/10.1056/NEJMoa1707914

Ridker, P. M., MacFadyen, J. G., Thuren, T., Everett, B. M., Libby, P., & Glynn, R. J. (2018). Modulation of the interleukin-6 signalling pathway and incidence rates of atherosclerotic events and all-cause mortality: Analyses from the CANTOS study. *European Heart Journal, 39*(38), 3499–3507. https://doi.org/10.1093/eurheartj/ehy389

Ridker, P. M., Rifai, N., Stampfer, M. J., & Hennekens, C. H. (2000). Plasma concentration of interleukin-6 and the risk of future myocardial infarction among apparently healthy men. *Circulation, 101*(15), 1767–1772. https://doi.org/10.1161/01.CIR.101.15.1767

Roshan, M. H. K., Tambo, A., & Pace, N. P. (2016). The role of TLR2, TLR4, and TLR9 in the pathogenesis of atherosclerosis. *International Journal of Inflammation, 2016*, Article 1532832. https://doi.org/10.1155/2016/1532832

Serhan, C. N., & Savill, J. (2005). Resolution of inflammation: The beginning programs the end. *Nature Immunology, 6*(12), 1191–1197. https://doi.org/10.1038/ni1276

Serhan, C. N., Chiang, N., & Van Dyke, T. E. (2008). Resolving inflammation: Dual anti-inflammatory and pro-resolution lipid mediators. *Nature Reviews Immunology, 8*(5), 349–361. https://doi.org/10.1038/nri2294

Singh, B., Cui, K., Eisa-Beygi, S., Zhu, B., Cowan, D. B., Shi, J., Wang, D.-Z., Liu, Z., Bischoff, J., & Chen, H. (2024). Elucidating the crosstalk between endothelial-to-

mesenchymal transition (EndoMT) and endothelial autophagy in the pathogenesis of atherosclerosis. *Vascular Pharmacology, 155*, Article 107368. https://doi.org/10.1016/j.vph.2024.107368

Singh, S., Anshita, D., & Ravichandiran, V. (2021). MCP-1: Function, regulation, and involvement in disease. *International Immunopharmacology, 101*, Article 107598. https://doi.org/10.1016/j.intimp.2021.107598

Tabas, I. (2010). The role of endoplasmic reticulum stress in the progression of atherosclerosis. *Circulation Research, 107*(7), 839–850. https://doi.org/10.1161/CIRCRESAHA.110.224766

Tabas, I., & Bornfeldt, K. E. (2016). Macrophage phenotype and function in different stages of atherosclerosis. *Circulation Research, 118*(4), 653–667. https://doi.org/10.1161/CIRCRESAHA.115.306256

Tall, A. R., & Yvan-Charvet, L. (2015). Cholesterol, inflammation and innate immunity. *Nature Reviews Immunology, 15*(2), 104–116. https://doi.org/10.1038/nri3793

Tardif, J.-C., Kouz, S., Waters, D. D., Bertrand, O. F., Diaz, R., Maggioni, A. P., Pinto, F. J., Ibrahim, R., Gamra, H., Kiwan, G. S., Berry, C., López-Sendón, J., Ostadal, P., Koenig, W., Angoulvant, D., Grégoire, J. C., Lavoie, M.-A., Dubé, M.-P., Rhainds, D., … Roubille, F. (2019). Efficacy and safety of low-dose colchicine after myocardial infarction. *New England Journal of Medicine, 381*(26), 2497–2505. https://doi.org/10.1056/NEJMoa1912388

Timmins, J. M., Ozcan, L., Seimon, T. A., Li, G., Malagelada, C., Backs, J., Backs, T., Bassel-Duby, R., Olson, E. N., Anderson, M. E., & Tabas, I. (2009). Calcium/calmodulin-dependent protein kinase II links endoplasmic reticulum stress with Fas and mitochondrial apoptosis pathways. *Journal of Clinical Investigation, 119*(10), 2925–2941. https://doi.org/10.1172/JCI38857

Wang, D., & DuBois, R. N. (2010). Eicosanoids and cancer. *Nature Reviews Cancer, 10*(3), 181–193. https://doi.org/10.1038/nrc2809

Xu, S., Liu, Y., Zhu, M., Chen, K., Xu, F., & Liu, Y. (2025). Global burden of atherosclerotic cardiovascular disease attributed to lifestyle and metabolic risks. *Science China Life Sciences, 68*(9), 2739–2754. https://doi.org/10.1007/s11427-025-2948-y

Xu, Y., Zhang, Y., & Li, X. (2022). NLRP3 inflammasome and atherosclerosis: Mechanisms and potential therapeutic targets. *Signal Transduction and Targeted Therapy, 7*(1), Article 251. https://doi.org/10.1038/s41392-022-01099-4

Zhang, H., Lui, K. O., & Zhou, B. (2024). Elucidating the crosstalk between endothelial-to-mesenchymal transition (EndoMT) and endothelial autophagy in the pathogenesis of atherosclerosis. *Pharmacological Research, 201*.